American Mineralogist, Volume 75, pages 1080–1091, 1990

A thermodynamic model for the enstatite-diopside join

TIBOR GASPARIK
Mineral Physics Institute, Department of Earth and Space Sciences, State University of New York at Stony Brook, Stony Brook, New York 11794, U.S.A.

ABSTRACT

A thermodynamic model for the enstatite-diopside join consistent with all experimental observations has been developed. Unlike previous models, this model reproduces exactly the phase relations determined by Carlson (1988) in the enstatite-rich portion of the join at 1 bar and 1295–1425 °C. The model fits the high-pressure data up to 60 kbar as well as previous models. However, only this model is consistent with the data at 100–152 kbar. Although the new model is similar in complexity to the models used before, the improvements were achieved by including second-order parameters related to the differences in heat capacity and compressibility. The model predicts the stability of all enstatite polymorphs, including the previously unrecognized stability of high clinoenstatite at temperatures below melting. The stability of orthopyroxene at 1 bar and high temperatures is confirmed. The ability of the model to predict the compositions of two coexisting pyroxenes at 100–160 kbar is essential for deciphering the mineral and chemical composition and the evolution of the Earth's upper mantle.

INTRODUCTION

In a series of recent papers, Carlson reported new data for the enstatite-diopside join at 1 bar and presented evidence for the reappearance of orthopyroxene at 1370–1445 °C (Carlson 1985, 1986, 1988, and Carlson et al., 1988). However, the subsequent thermodynamic models did not succeed in reproducing the experimentally observed stability field of orthopyroxene at 1 bar and high temperatures. The model of Carlson and Lindsley (1988) was the first attempt to include protoenstatite. The model does not reproduce the experimentally determined shape of the orthopyroxene stability field at 1 bar and high temperatures, and has some peculiar properties at high temperatures that limit the use of the model in the pyroxene quadrilateral. Davidson et al. (1988) pointed out the problems with that model and proposed a new model that fits the data in the pressure-temperature range important for geothermometry and ignored the high-temperature stability of orthopyroxene at 1 bar and the data at pressures above 30 kbar. This study presents a thermodynamic model capable of reproducing all experimentally observed phase relations, including the correct shape of the orthoenstatite stability field at 1 bar and high temperatures, the data of Brey and Huth (1984) and Nickel and Brey (1984) at 40–60 kbar, the data of Yamada and Takahashi (1984) at 50–100 kbar, and the data of Gasparik (1989) at 100–152 kbar.

THERMODYNAMIC MODEL

The model is similar to that of Lindsley et al. (1981), which was used in many subsequent modeling studies. Carlson and Lindsley (1988) expanded this model to include protoenstatite. The main difference in the present model is in the addition of the second-order parameters related to the differences in heat capacity and compressibility, which produce curved end-member boundaries; until now, only the first-order parameters (ΔH, ΔS, ΔV) were used, resulting in straight boundaries.

Pyroxenes on the enstatite-diopside join ($Mg_2Si_2O_6$-$CaMgSi_2O_6$) usually belong to one of the three solid solutions: protopyroxene (Ppx), the solution of protoenstatite (PEn) and protodiopside (PDi); orthopyroxene (Opx), the solution of orthoenstatite (OEn) and orthodiopside (ODi); and clinopyroxene (Cpx), the solution of clinoenstatite (CEn) and clinodiopside (CDi). Pigeonite (Pig) is the Ca-poor clinopyroxene at temperatures and pressures where immiscibility produces two clinopyroxene phases. Pigeonite has the $C2/c$ structure at high temperatures and is likely to belong to the same solid solution as the Ca-rich clinopyroxene (Lindsley et al., 1981). It is possible to write six reactions among the end-members of these solid solutions (of which only four reactions are independent). The equilibrium conditions are

$$\text{OEn} = \text{CEn}, \qquad RT \ln a_{\text{CEn}} - RT \ln a_{\text{OEn}} + \Delta G(A) = 0, \tag{A}$$

$$\text{ODi} = \text{CDi}, \qquad RT \ln a_{\text{CDi}} - RT \ln a_{\text{ODi}} + \Delta G(B) = 0, \tag{B}$$

$$\text{PEn} = \text{CEn}, \qquad RT \ln a_{\text{CEn}} - RT \ln a_{\text{PEn}} + \Delta G(C) = 0, \tag{C}$$

$$\text{PDi} = \text{CDi}, \qquad RT \ln a_{\text{CDi}} - RT \ln a_{\text{PDi}} + \Delta G(D) = 0, \tag{D}$$

$$\text{PEn} = \text{OEn}, \qquad RT \ln a_{\text{OEn}} - RT \ln a_{\text{PEn}} + \Delta G(E) = 0, \tag{E}$$

0003–004X/90/0910–1080$02.00

$$\text{PDi} = \text{ODi}, \qquad \text{(F)}$$
$$RT \ln a_{\text{ODi}} - RT \ln a_{\text{PDi}} + \Delta G(F) = 0,$$

where

$$\Delta G_{T,P} = \Delta H^\circ_{970} - T\Delta S^\circ_{970} - \int_{970}^{T}\int_{970}^{T} \Delta C_p/T \, dT dT + \int_1^P \Delta V_{T,P} \, dP.$$

This expression from Gasparik and Newton (1984) can be simplified to

$$\Delta G = \Delta H^\circ - T\Delta S^\circ - cT^{1.5} + P\Delta V - bP^2,$$

where

$$\Delta C_p = 0.75cT^{0.5},$$

$$\int_{970}^{T}\int_{970}^{T} \Delta C_p/T \, dT dT = 15108c - 46.72cT + cT^{1.5},$$

$$\Delta H^\circ = \Delta H^\circ_{970} - 15108c,$$

$$\Delta S^\circ = \Delta S^\circ_{970} - 46.72c,$$

$$\int_1^P \Delta V_{T,P} \, dP = P\Delta V^\circ_T - 0.5\,\Delta(\beta V^\circ_T)P^2 = P\Delta V^\circ_T - bP^2.$$

In addition to the first-order parameters, ΔH, ΔS, and ΔV, the expression for ΔG includes two second-order parameters c, expressing the heat capacity differences, and b, expressing the differences in compressibilities between the end-members in Reactions A–F. All parameters reported in this study are in joules (J), kelvins (K), and bars (bar).

The activities of the pyroxene components were approximated by the Redlich-Kister equation (Redlich and Kister, 1948; Gasparik, 1984):

$$RT \ln a_{\text{En}} = RT \ln X_{\text{En}} + A_G X^2_{\text{Di}} + B_G(4X^3_{\text{Di}} - 3X^2_{\text{Di}}),$$

$$RT \ln a_{\text{Di}} = RT \ln X_{\text{Di}} + A_G X^2_{\text{En}} + B_G(3X^2_{\text{En}} - 4X^3_{\text{En}}),$$

where $A_G = A_H - A_S T + A_V P$, and $B_G = B_H - B_S T + B_V P$. The A_G parameter produces a symmetric solution; B_G introduces asymmetry. The Redlich-Kister parameters are directly related to the more commonly used Margules parameters: $W_{12} = A_G - B_G$, and $W_{21} = A_G + B_G$. In the present model, as in most of the previous models, excess entropy terms were not used (or needed) because the enstatite-diopside solutions are likely to have negligible disorder.

Solution modeling

Modeling procedures commonly employed involve simultaneous fitting of all experimental data using least-squares regression (Lindsley et al., 1981) or linear programming (Carlson and Lindsley, 1988). The result is a set of parameters that can be used with the corresponding thermodynamic model to calculate the experimentally observed phase relations. One major problem in this approach is that the relationship between the phase compositions and the model parameters is nonlinear; a small error in the input compositions can sometimes result in very large errors in ΔG, and, at the other extreme, some fine details in the experimentally observed phase relations can be associated with very small changes in ΔG. Lindsley et al. (1981) suggested a solution to this problem: the input compositions in the least-squares regression are adjusted within acceptable limits until all residuals become negligible. Similar adjustments of the input compositions are also required in the linear programming technique to make the solution possible or to alleviate constraints that are too rigid (Carlson and Lindsley, 1988). Although these techniques work in most cases, they have not been completely successful in modeling the enstatite-diopside join.

The procedure used in this study was the reverse of the previous approach. Instead of adjusting the experimental compositions, the model parameters were adjusted; each time an adjustment was made, selected compositions were calculated with the newly modified model and compared with the compositions constrained by experiments. It was observed that each parameter dominates a certain aspect of a phase diagram and has only a minor effect on the rest. This allows sequential refinement of the parameters, if the sequence is chosen correctly. The final step involved iteration, which smoothed out the remaining discrepancies between the calculated and the experimentally determined compositions.

The enstatite-diopside join is particularly suitable for the approach described because the highly detailed experimental study of Carlson (1988) at 1 bar provides narrow constraints on the enthalpy and entropy parameters, minimizing the need to consider initially the high-pressure data. In some cases, the parameters from the previous models served as convenient starting points for their further refinement. Most of the experimental data used in the fitting procedure were summarized by Carlson and Lindsley (1988, their Table 1).

The enstatite-diopside join at 1 bar

The modeling procedure was begun by fitting the two-clinopyroxene solvus, which is mainly constrained by Carlson's (1988) data at 1 bar in the temperature range 1295–1375 °C, with the result $A_H(\text{Cpx}) = 29270$, and $B_H(\text{Cpx}) = -2800$. At 1295 °C, the resulting parameters predicted pigeonite with 16.86 mol% diopside coexisting with clinopyroxene containing 73.33% diopside (Fig. 1).

Although immiscibility was not observed in orthopyroxene and protopyroxene because of their limited compositional range, these solutions are not likely to be ideal, considering the large miscibility gap in clinopyroxene. Thus, although the experimental data could be equally well satisfied with an ideal orthopyroxene or protopyroxene, the assignment of a reasonable amount of nonideal-

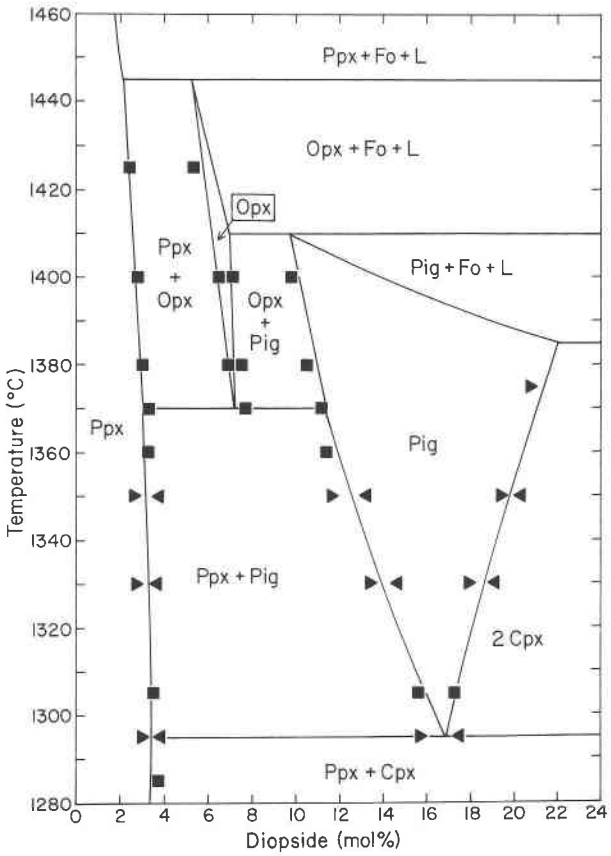

Fig. 1. Calculated temperature-composition phase diagram for the enstatite-rich portion of the enstatite-diopside join at 1 bar and the experimental data of Carlson (1988). Triangles indicate reversals, squares correspond to synthesis experiments.

ity to both solutions would result in more realistic values for the parameters in Reactions B, D, and F. For both orthopyroxene and protopyroxene, the value of A_G was set at 20 kJ, as proposed by Davidson et al. (1988).

At 1295–1370 °C, the enstatite-rich compositions produced coexisting protopyroxene and pigeonite (Fig. 1). Carlson's (1988) data indicate that the Ca content of the pigeonite and, to a smaller degree, of the coexisting protopyroxene decreases with increasing temperature. The same trend was observed above 1370 °C for the coexisting orthopyroxene and pigeonite at higher Ca contents and for the coexisting protopyroxene and orthopyroxene at lower Ca contents. These trends required that the end-member reactions OEn = CEn, PEn = CEn, and PEn = OEn all be located at higher temperatures than the phase relations at 1295–1425 °C. This contradicted the experimentally determined protoenstatite-orthoenstatite transition at 985 (±10) °C (Atlas, 1952). The contradiction can be resolved only if the protoenstatite-orthoenstatite boundary appears at 1 bar at two different temperatures. This can be achieved by introducing a ΔC_P term that causes a change in the slope of the protoenstatite-orthoenstatite boundary with increasing temperature from positive to negative. The anomalous heat capacity was assigned to protoenstatite, and thus appears only in Reactions C and E. The magnitude of the ΔC_P term affects the size, shape, and composition of the high-temperature stability field of orthopyroxene. After several trials with smaller ΔC_P terms, the parameter $0.6T^{1.5}$ (resulting from the double integral of ΔC_P) produced the most satisfactory fit.

The protopyroxene-pigeonite equilibrium at 1295–1370 °C and the protopyroxene-clinopyroxene equilibrium at 1005–1295 °C are controlled by Reactions C and D. Reaction C primarily controls the pigeonite limb, and Reaction D the protopyroxene limb of the protopyroxene-pigeonite solvus. The clinopyroxene limb of the protopyroxene-clinopyroxene solvus is primarily controlled by the miscibility gap in the clinopyroxene solution and only to a small extent by Reaction C. Although the temperature range of the protopyroxene-pigeonite stability is quite small, the temperature dependence of the pigeonite composition was determined by Carlson (1988) well enough to constrain $\Delta H°$(C) and $\Delta S°$(C); both parameters were adjusted until the pigeonite limb of the protopyroxene-pigeonite solvus was placed at 16.86 mol% diopside at 1295 °C and thus intersected the two-clinopyroxene solvus at that temperature. At the same time, the pigeonite limb at 1370 °C had to be placed at a composition close to 11 mol% diopside to satisfy the data (Fig. 1). The following parameters place this composition at 11.31% diopside: $\Delta G°(C) = -14475 + 33.6T - 0.6T^{1.5}$. The parameters for Reaction D were obtained by fitting the compositions of protopyroxene at 1005–1370 °C. The values were finalized in the subsequent iterations by placing the protopyroxene-orthopyroxene-clinopyroxene equilibrium at 1005 °C: $\Delta G°(D) = -11920 - 7T$.

The next step was to fit the compositions of coexisting orthopyroxene and pigeonite at 1370–1400 °C (Fig. 1). This equilibrium is controlled by Reactions A and B. The parameters for Reaction A are constrained by Reaction C, determined in the previous step, and by Reaction E which was experimentally located at 980 °C (Atlas, 1952). This left only one adjustable parameter for Reaction A, which was found by trial and error. The parameter varied during modeling was $\Delta S°$(E); for each value of $\Delta S°$(E), $\Delta H°(E) = 1253\Delta S°(E)$. The parameters for Reaction A were then calculated: $\Delta G°(A) = \Delta G°(C) - \Delta G°(E)$. By adjusting the parameters for Reaction B, the pigeonite limb was placed at the composition 11.31% diopside at 1370 °C to intersect the protopyroxene-pigeonite solvus. The composition of the coexisting orthopyroxene and the shape of the orthopyroxene stability field depended on the value of $\Delta S°$(E). The closest agreement with the experimental data was found using the following parameters:

$$\Delta G°(E) = -17932 + 35.55T - 0.6T^{1.5},$$
$$\Delta G°(A) = 3457 - 1.95T,$$
$$\Delta G°(B) = -32845 + 12T.$$

In this step, one of the parameters for Reaction B was selected, in this case $\Delta S°$, and only the enthalpy param-

eter was adjusted to place the pigeonite limb at 1370 °C and 11.31% diopside. In the subsequent iterations, the parameters for Reaction B were finalized by fitting the orthopyroxene limb of the orthopyroxene-clinopyroxene solvus at temperatures below 1005 °C.

The calculated phase relations for the enstatite-diopside join at 1 bar are shown in Figures 1 and 2a. Figure 1 compares favorably with the hand-drawn phase diagram of Carlson (1988, his Fig. 6).

The orthopyroxene-clinopyroxene equilibrium at high pressures

The only data on the two-clinopyroxene solvus at high pressures are the compositions of coexisting orthopyroxene, pigeonite, and clinopyroxene at 15 kbar and 1465 °C (Schweitzer, 1982). However, these experimental results allow a range of compositions for the coexisting phases and thus do not provide narrow constraints on the high-pressure behavior of the two-clinopyroxene solvus. The orthopyroxene-clinopyroxene equilibrium data place indirect constraints on the two-clinopyroxene solvus, because the clinopyroxene limb of the orthopyroxene-clinopyroxene solvus is primarily controlled by immiscibility in the clinopyroxene solution and only to a much lesser extent by Reaction A. Most of the high-pressure data give information on the compositions of coexisting orthopyroxene and clinopyroxene. These data at pressures up to 60 kbar can be reproduced with the existing thermodynamic models without major problems.

Gasparik (1989) reported new data on the coexisting orthopyroxene and clinopyroxene at 100 kbar (Fig. 2n) that show that the temperature dependence of the clinopyroxene limb at this pressure was much stronger than predicted by any of the existing thermodynamic models. Apparently, the relatively small pressure range of the previous data did not constrain adequately the high-pressure dependence of the two-clinopyroxene solvus; here, this dependence was modeled from the data at 100 kbar and Schweitzer's (1982) data at 15 kbar.

The compositions of the coexisting pigeonite and clinopyroxene were fitted at 15 kbar and 1465 °C by selecting such values for A_V and B_V of clinopyroxene to obtain compositions in agreement with Schweitzer's (1982) data. The ΔV(A) value was then adjusted until the composition of the clinopyroxene coexisting with orthopyroxene was identical to the composition of clinopyroxene coexisting with pigeonite at 1465 °C. The value of ΔV(B) was simultaneously adjusted to keep the orthopyroxene composition within the experimental range. Then the orthopyroxene-clinopyroxene solvus was calculated at 100 kbar and compared with the experimental data. This procedure was repeated with different values of A_V and B_V until the temperature dependence of the clinopyroxene limb at 100 kbar was consistent with the experimental observations. The goal was to place this limb at 1650 °C, 60 mol% diopside, and 1750 °C, 50 mol% diopside. The greater temperature dependence of the clinopyroxene limb was achieved mainly by using a larger value for B_V than in the previous models, with the result $A_G = 29270 - 0.03P$, and $B_G = -2800 + 0.04P$. These excess parameters produce a solvus that is asymmetrically skewed toward enstatite at 1 bar and that then becomes symmetric at 70 kbar, and again asymmetric but skewed toward diopside at higher pressures.

It became apparent during the fitting procedure that, by themselves, ΔV parameters in Reactions A and B would not be sufficient to express the high-pressure behavior of the orthopyroxene-clinopyroxene solvus. The reason is that the Ca content of orthopyroxene coexisting with clinopyroxene increases between 1 bar and 15 kbar but decreases at higher pressures. Therefore, compressibility parameters were required to express the pressure dependence of the orthopyroxene composition (Reaction B) and to place the clinopyroxene limb of the orthopyroxene-clinopyroxene solvus at 100 kbar in agreement with the data (Reaction A). The most satisfactory fit was achieved with the following parameters:

$$\Delta G(\text{A}) = 3457 - 1.95T + 0.038P + 1.7 \times 10^{-7}P^2,$$

$$\Delta G(\text{B}) = -32845 + 12T + 0.09P - 40 \times 10^{-7}P^2.$$

The calculated temperature-composition phase diagrams for the enstatite-diopside join at various pressures are in Figure 2. Also plotted are experimental data, taken mostly from Table 1 of Carlson and Lindsley (1988), which allow the comparison between the model and the experimental observations.

Protopyroxene at high pressures

The parameters based on the Carlson's (1988) data limit the stability of protopyroxene at 1 bar to the temperature range 980–1604 °C. The success of the present model depended on its consistency with existing experimental data on the high-pressure stability of protopyroxene.

The most important constraints on the stability of protopyroxene are provided by the experimental data on the end-member protoenstatite-orthoenstatite boundary at high pressures (Fig. 3). The boundary was determined at 1200–1350 °C by Kushiro et al. (1968) and at 1000–1300 °C by Anastasiou and Seifert (1972). The results of both studies are consistent with each other and with a straight line passing through 975 °C at 1 bar, in agreement with Atlas (1952). Thus, these data do not indicate that the boundary curves and returns to 1 bar at 1604 °C, as required by the model. However, a linear extrapolation of the boundary to higher temperatures is inconsistent with the determination of the boundary by Boyd et al. (1964) at temperatures between 1550 °C and the solidus. Chen and Presnall (1975) attempted to resolve this discrepancy by conducting additional experiments at temperatures above 1300 °C. Although they obtained a reversal at 8 kbar and 1313–1417 °C consistent with the low-temperature data, the experiments at higher temperatures produced orthoenstatite, in violation of a straight protoenstatite-orthoenstatite boundary.

In order for the model to be consistent with all exper-

imental observations, it was necessary to find pressure-dependent parameters that would produce an approximately straight protoenstatite-orthoenstatite boundary in the temperature range 980–1300 °C and a sharp curve at higher temperatures. A simple ΔV term combined with the ΔH, ΔS, and ΔC_P parameters derived from the data at 1 bar produced a symmetric curve with the pressure maximum at the midpoint between 980 and 1604 °C. This symmetry was preserved even after introducing terms for compressibility or thermal expansion. In contrast, the experimental observations require an asymmetric curve with the pressure maximum around 1450 °C. This was achieved by introducing pressure dependence to the ΔC_P parameter, with the result

$$\Delta G(\mathrm{E}) = -17932 + 35.55T - 0.6T^{1.5}(1 - 633 \times 10^{-8}P) - 0.32P.$$

The same pressure dependence of heat capacity was assigned to Reaction C:

$$\Delta G(\mathrm{C}) = \Delta G(\mathrm{E}) + \Delta G(\mathrm{A}),$$
$$\Delta G(\mathrm{C}) = -14475 + 33.6T - 0.6T^{1.5}(1 - 633 \times 10^{-8}P) - 0.282P + 1.7 \times 10^{-7}P^2.$$

The calculated protoenstatite-orthoenstatite boundary and the corresponding experimental data are in Figure 3. The boundary is consistent with the stability of orthoenstatite indicated by the experimental results of Chen and Presnall (1975) and even with the data of Boyd et al. (1964). Boyd et al. (1964) determined the protoenstatite-orthoenstatite boundary at 1550 °C; however the data at higher temperatures apply to the orthoenstatite-clinoenstatite boundary, where clinoenstatite is most likely identical to high clinoenstatite (Perrotta and Stephenson, 1965). Both protoenstatite and high clinoenstatite quench as low clinoenstatite and thus cannot be distinguished in the experimental products.

To complete the model, it was necessary to assign pressure dependencies to Reactions D and F. Theoretically, this could be accomplished by fitting the data of Biggar (1988) for protopyroxene coexisting with clinopyroxene or orthopyroxene. However, the protopyroxene composition is rather insensitive to pressure, and fitting the data exactly would require unrealistically large ΔV parameters. Thus the ΔV values were assigned arbitrarily by assuming zero pressure dependency for Reaction D, following Carlson and Lindsley (1988) and Davidson et al. (1988). The resulting protopyroxene compositions have slightly larger Ca contents than those determined by Biggar (1988), but the boundary between orthopyroxene and protopyroxene + clinopyroxene is in agreement (Fig. 3).

The calculated temperature-composition phase diagrams for the enstatite-diopside join involving protoen-

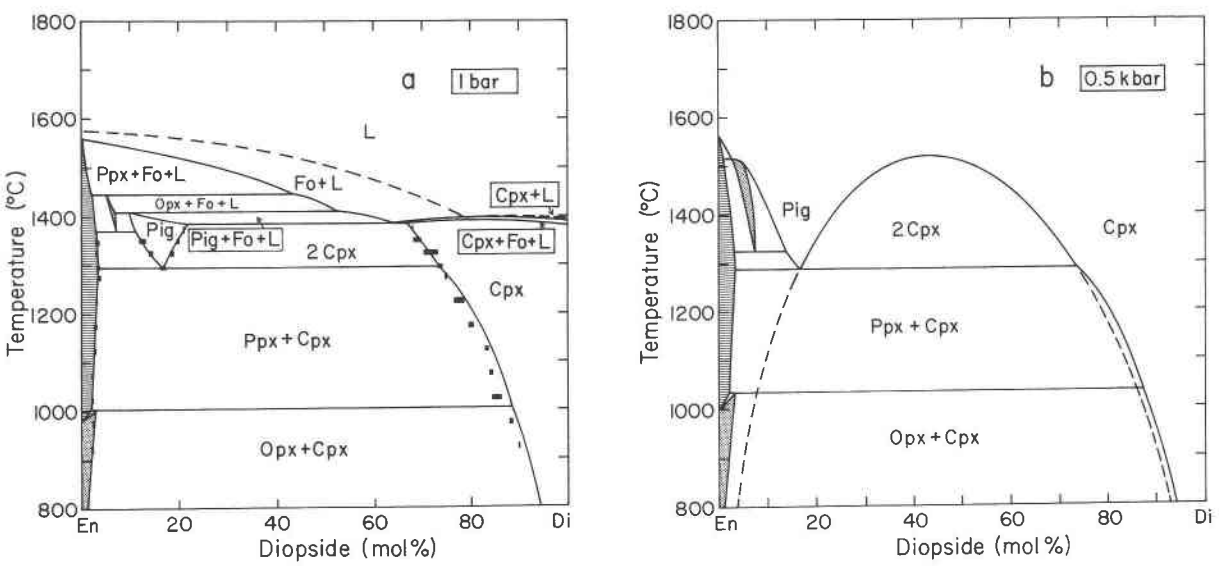

Fig. 2. Calculated temperature-composition phase diagrams for the enstatite-diopside join. Solid bars indicate the compositional ranges allowed by the experimental data listed in Table 1 of Carlson and Lindsley (1988), including the data of Warner and Luth (1974), Mori and Green (1975), Lindsley and Dixon (1976), Perkins and Newton (1980), Schweitzer (1982), Brey and Huth (1984), Nickel and Brey (1984), and Carlson (1986, 1988). Additional data included are from Biggar (1988), Mori and Green (1976), and Gasparik (1989). Ruled areas indicate the stability field of protopyroxene, dotted pattern shows the stability of orthopyroxene. Dashed lines are metastable extensions of the two-clinopyroxene solvus. Boxes in Figure 2n indicate the range of the observed compositions and the experimental uncertainty in temperature.

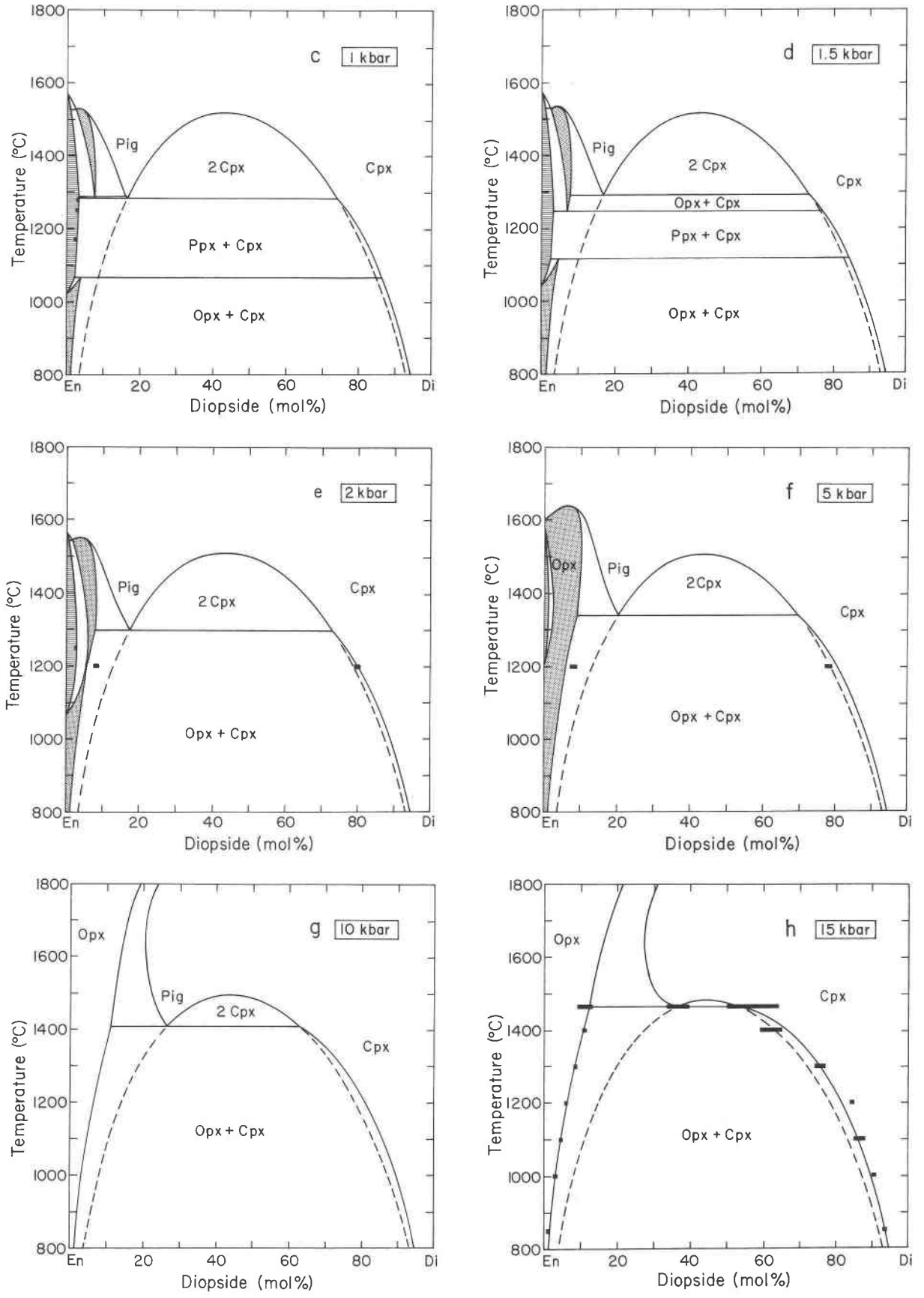

Fig. 2.—*Continued.*

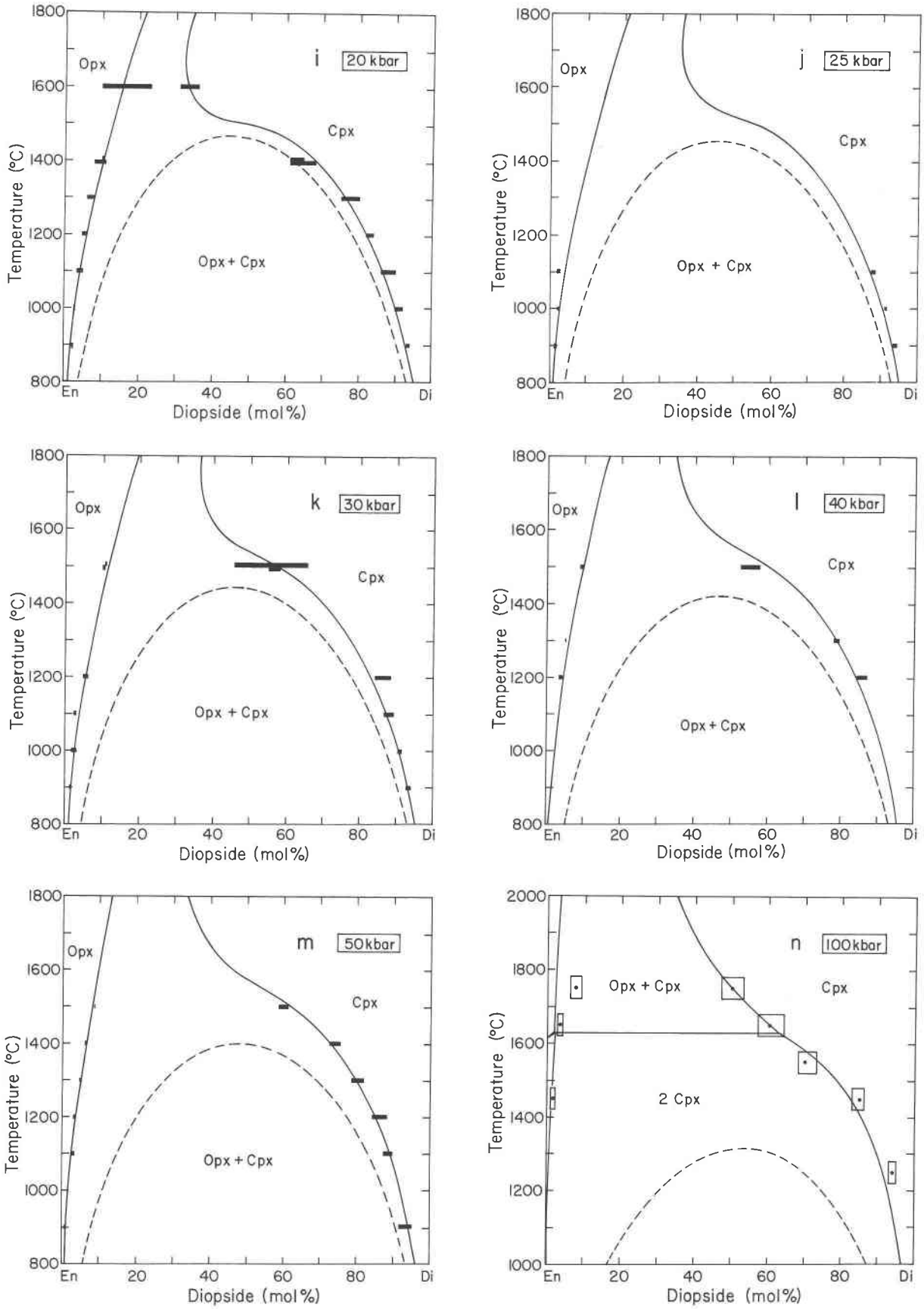

Fig. 2.—*Continued.*

statite are shown in Figures 2a–f. With increasing pressure, the stability fields of protopyroxene + pigeonite and protopyroxene + clinopyroxene narrow. The protopyroxene-pigeonite solvus disappears at pressures slightly above 1 kbar, and a second high-temperature orthopyroxene-clinopyroxene solvus forms at higher pressures (Fig. 2d). The protopyroxene-clinopyroxene solvus is eliminated at 1.8 kbar. Protopyroxene coexists with orthopyroxene only at 1.8–8.5 kbar, and is metastable at higher pressures.

Discussion

The thermodynamic model derived above is consistent with most of the experimental data in the pressure range 0–100 kbar and temperature range 850–1750 °C. It reproduces exactly the phase relations involving high-temperature orthopyroxene at 1 bar and, at the same time, fits the high-pressure data as well as any of the previous models. However, there are still some discrepancies between the model and the experimental data.

A discrepancy was observed at 1 bar between the data and the calculated clinopyroxene limbs of the orthopyroxene-clinopyroxene and protopyroxene-clinopyroxene solvi at 900–1200 °C. The data indicate higher enstatite solubilities in clinopyroxene than the model predicts. The same kind of discrepancy was produced by the model of Carlson and Lindsley (1988); in that model, however, the authors reduced the discrepancy by increasing the asymmetry of the two-clinopyroxene solvus. This resulted in a less satisfactory fit to the pigeonite compositions at 1295–1350 °C, whereas the improvement to the clinopyroxene compositions at lower temperatures was marginal. In addition, this compromise also worsened the fit to the high-pressure data. The discrepancy seems to be limited to the data at 1 bar obtained with the flux, which was present in minor amounts in all crystalline phases; thus, the discrepancy could have resulted from an incorrect projection of the pyroxene compositions to the enstatite-diopside join.

A number of discrepancies at high pressures reflect internal inconsistencies among the data, which cannot be satisfied with any model. However, small systematic discrepancies in the compositions of the Ca-rich clinopyroxene at 1400 °C and higher temperatures may have resulted from fitting exactly the data of Schweitzer (1982); Carlson and Lindsley (1988) compromised by lowering the temperature for the three coexisting pyroxenes from 1465 to 1436 °C. The improvement however was minor and did not seem to warrant the compromise.

Carlson's (1988) data place unusually strong constraints on the enthalpy and entropy parameters of the end-member reactions. Whereas the parameters for the diopside end-member reactions are model dependent, the parameters for the enstatite end-member reactions are likely to be very close to the true thermodynamic values because the crucial experimental constraints include enstatite-rich compositions. The data allow refinement of

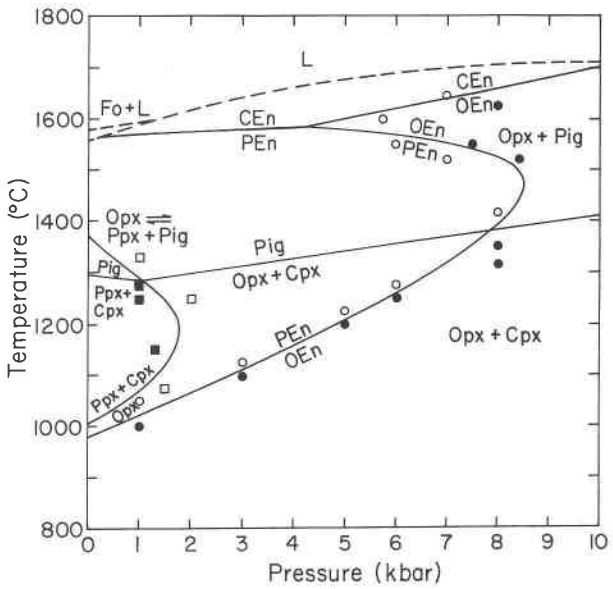

Fig. 3. Temperature-pressure phase diagram for the enstatite-diopside join showing the calculated univariant phase boundaries and the corresponding experimental data. Round symbols indicate the data of Boyd et al. (1964), Anastasiou and Seifert (1972), and Chen and Presnall (1975) for the enstatite composition. Squares represent the data of Biggar (1988) for the enstatite-diopside compositions.

the corresponding enthalpy differences to a few joules; such precision is currently not possible in the calorimetric measurements. The potential application of the thermochemical data is further hampered by the metastability or limited stability for most of the participating end-member phases, by the uncertainty in the extrapolation of the measurements to high temperatures, and by the small differences in the thermochemical values between the phases in the end-member reactions.

The parameters for Reaction A are particularly well constrained by the data at 1 bar and surprisingly close to the values obtained by Lindsley et al. (1981). The values for ΔH(A) are consistently lower in all existing models than the value of 8.4 ± 4.2 kJ/mol estimated by Newton et al. (1979) from the enthalpy of solution measurements.

The volume parameters in the model are in broad agreement with the measured molar volumes. The unit-cell volumes reported by Smith (1969) allow the determination of ΔV for the protoenstatite-orthoenstatite transition of −0.214 J/bar at 1 bar and 25 °C, which compares favorably with the model value of −0.32 J/bar. Nickel and Brey (1984) proposed that the difference between the unit-cell volumes of orthoenstatite and clinoenstatite, estimated from the molar volumes of the enstatite-diopside clinopyroxenes reported by Newton et al. (1979), is in the range of −0.01 to +0.07 J/bar, which is consistent with the model value of +0.038 J/bar.

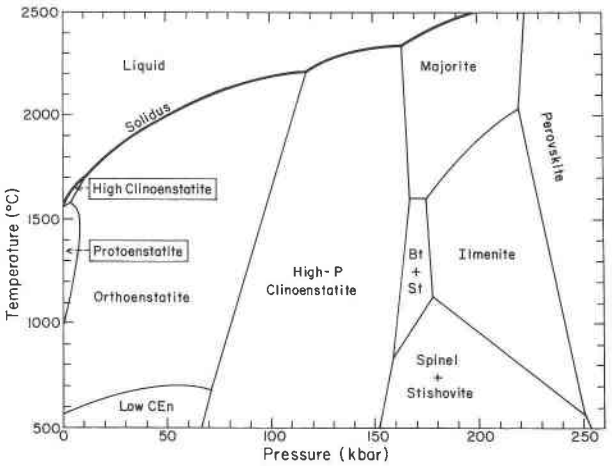

Fig. 4. Temperature-pressure phase diagram for the $MgSiO_3$ system. Melting curve after Boyd et al. (1964) and Presnall and Gasparik (1990). Post-pyroxene phase relations based on Gasparik (1990). Abbreviations: Bt = Mg_2SiO_4 beta phase, St = stishovite.

Additional phase relations on the enstatite-diopside join

Grover (1972) demonstrated the stability of low clinoenstatite ($P2_1/c$) by obtaining reversals of the transition of orthoenstatite to low clinoenstatite under hydrostatic conditions at 2 and 4 kbar using $MgCl_2 \cdot H_2O$ as a flux. The resulting phase boundary was described by the equation T(°C) = 566 + 4.5P(kbar). A linear extrapolation of this boundary to high pressures predicts the stability of low clinoenstatite at higher temperatures than the earlier high-pressure studies by Sclar et al. (1964) and Boyd and England (1965), both conducted in solid-media devices. Shear stresses common in such devices favor the metastable formation of low clinoenstatite from orthoenstatite (Riecker and Rooney, 1967) and thus cannot explain the discrepancy. Yamamoto and Akimoto (1977) also reported orthoenstatite forming under presumably hydrostatic conditions at lower temperatures than the linear extrapolation of the Grover's boundary would allow. The experimental observations imply that the boundary separating orthoenstatite and low clinoenstatite curves to lower temperatures at high pressures (Fig. 4). This is not surprising, considering the small ΔV of the transition (−0.003 J/mol, Stephenson et al., 1966); even a small difference in compressibilities could produce a large curvature in the boundary.

Perrotta and Stephenson (1965) observed that low clinoenstatite transformed reversibly to a different phase at 995(±5) °C and named the new phase high clinoenstatite. Smith (1969) suggested that the structure of the new phase was $C2/c$. It is very likely that this high clinoenstatite is the end-member of the solution between $C2/c$ enstatite and $C2/c$ diopside, for which the present model predicts a limited stability below the solidus (Fig. 3). The following parameters were calculated from the temperature of the low CEn–high CEn transition of 995 °C (1 bar), from the temperature of the OEn–low CEn transition of 566 °C (and the suggested curved extrapolation to high pressures), and from the parameters of the OEn–high CEn transition derived in this study:

OEn = low CEn

$$\Delta G = -1921 + 2.29T - 0.011P + 10^{-7}P^2,$$

high CEn = low CEn

$$\Delta G = -5378 + 4.24T - 0.049P - 0.7 \times 10^{-7}P^2.$$

The resulting ΔV (−0.011 J/bar) for the transition of orthoenstatite to low clinoenstatite is close to the value of −0.003 J/bar measured at 1 bar (Stephenson et al., 1966). The model ΔV (−0.049 J/bar) for the transition between high and low clinoenstatite is similar to the value of −0.04 J/bar resulting from the measurements of Smyth (1974, his Figure 3) on high and low clinohypersthene.

The $MgSiO_3$ phase relations are further complicated by the observation of a transition from orthoenstatite to clinoenstatite at high pressures and temperatures (Yamamoto and Akimoto, 1977). Pacalo and Gasparik (1990) reversed this transition at 900–1700 °C (Fig. 4). Presnall and Gasparik (1990) also located the triple point for coexisting orthoenstatite, clinoenstatite, and melt at 2230 °C and 119 kbar. These experimental observations are consistent with a boundary given by the equation P(kbar) = 0.031T(°C) + 50. The slope of this boundary is much smaller than that for the boundary between orthoenstatite and low clinoenstatite determined by Grover (1972); thus, it is unlikely that the clinoenstatite at both boundaries is the same phase, despite the fact that the quench products are identical. Pacalo and Gasparik (1990) suggested that the clinoenstatite phase stable at high pressures and temperatures is a new high-pressure polymorph, high-pressure clinoenstatite, possibly an analogue of $Mg_2Ge_2O_6$ clinopyroxene (Ross and Navrotsky, 1988). Gasparik (1989) suggested the value of −0.2 J/bar for ΔV of the transition of orthoenstatite to high-pressure clinoenstatite, based on the similar ΔV (−0.234 J/bar) for the transition between orthopyroxene and clinopyroxene in the system $Mg_2Ge_2O_6$, resulting in the following parameters: $\Delta G = 8300 + 6.2T - 0.2P$. These parameters were used to calculate the two-clinopyroxene solvus in Figure 2n. The complete phase diagram for the $MgSiO_3$ system is in Figure 4.

The phase relations on the enstatite-diopside join at 1650 °C and pressures higher than 100 kbar were reported by Gasparik (1990). Two coexisting clinopyroxenes are stable to 156 kbar. At 156 kbar, the diopsidic pyroxene is replaced with a new high-pressure phase, the CM phase. Garnet with a composition close to $En_{80}Di_{20}$ (mol%) forms on the join at 163 kbar. The CM phase reacts to form garnet and perovskite ($CaSiO_3$) at 176 kbar. The Ca content of the garnet coexisting with the $CaSiO_3$ perovskite decreases rapidly with increasing pressure; ultimately the garnet reacts to form $MgSiO_3$ ilmenite and $CaSiO_3$ pe-

rovskite at 186 kbar. The $MgSiO_3$ ilmenite transforms to perovskite at 230 kbar; two coexisting perovskites are likely to be stable throughout the lower mantle.

Summary

This study presents a new thermodynamic model for the enstatite-diopside join that is consistent with all experimental observations. The phase relations on the enstatite-diopside join include five pyroxene solid solutions with ten end-members: orthopyroxene (OEn–ODi), protopyroxene (PEn–PDi), low clinopyroxene (low CEn–low CDi), high clinopyroxene (high CEn–high CDi), and high-pressure clinopyroxene (high-P CEn–high-P CDi). Following is the summary of all parameters (J, K, bar):

$$A_G(\text{high Cpx}) = 29270 - 0.03P,$$
$$B_G(\text{high Cpx}) = -2800 + 0.04P,$$
$$A_G(\text{Opx}) = A_G(\text{Ppx}) = A_G(\text{high-P Cpx}) = 20000,$$

OEn = high CEn,
$$\Delta G = 3457 - 1.95T + 0.038P + 1.7 \times 10^{-7}P^2,$$

ODi = high CDi,
$$\Delta G = -32845 + 12T + 0.09P - 40 \times 10^{-7}P^2,$$

PEn = high CEn,
$$\Delta G = -14475 + 33.6T - 0.6T^{1.5}(1 - 633 \times 10^{-8}P) - 0.282P + 1.7 \times 10^{-7}P^2,$$

PDi = high CDi,
$$\Delta G = -11920 - 7T,$$

PEn = OEn,
$$\Delta G = -17932 + 35.55T - 0.6T^{1.5}(1 - 633 \times 10^{-8}P) - 0.32P,$$

PDi = ODi,
$$\Delta G = 20925 - 19T - 0.09P + 40 \times 10^{-7}P^2,$$

OEn = high-P CEn,
$$\Delta G = 8300 + 6.2T - 0.2P,$$

ODi = high-P CDi,
$$\Delta G = -15000 + 12T + 0.29P - 40 \times 10^{-7}P^2,$$

OEn = low CEn,
$$\Delta G = -1921 + 2.29T - 0.011P + 10^{-7}P^2,$$

high CEn = low CEn,
$$\Delta G = -5378 + 4.24T - 0.049P - 0.7 \times 10^{-7}P^2.$$

These parameters were used to evaluate the thermodynamic properties of the pyroxene end-members at 970 K (Table 1). The reference temperature of 970 K was chosen for several reasons: the enthalpy measurements are usually conducted at this temperature, the temperature is within the range of the heat-capacity measurements, and it is close to the temperature range of the phase-equilibrium experiments. The parameters for orthoenstatite and diopside (high clinodiopside) were evaluated from the enthalpy, heat-capacity, and unit-cell volume measurements; the parameters for the remaining end-members were calculated from the differences given in the end-member reactions. The only end-member other than orthoenstatite and diopside for which thermochemical measurements are available is low clinoenstatite. The values at 298 K from Robie et al. (1978) extrapolated to 970 K with the heat-capacity equations of Berman and Brown (1985) yield the value of −71.1 kJ/mol for the enthalpy of formation from oxides, and 383.7 J/molK for the entropy, in close agreement with the calculated parameters in Table 1.

Table 1. Thermodynamic properties of pyroxene end-members

Phase	$\Delta H^o_{f,970}$ (kJ/mol)	S^o_{970} (J/mol·K)	V^o_{970} (J/bar)
Orthoenstatite	−69.5[a]	386.2[c]	6.400[d]
Protoenstatite	−60.63	393.72	6.720
Low clinoenstatite	−71.42	383.91	6.389
High clinoenstatite	−66.04	388.15	6.438
High-P clinoenstatite	−61.20	380.0	6.200
Orthodiopside	−113.55	408.3	6.670
Protodiopside	−134.48	389.3	6.760
High clinodiopside	−146.4[b]	396.3[c]	6.760[e]
High-P clinodiopside	−128.55	396.3	6.960

Note: [a] = Enthalpy of formation from oxides at 970 K, based on Kiseleva et al. (1979), Chatillon-Colinet et al. (1983), and Brousse et al. (1984); [b] = Charlu et al. (1978); [c] = Krupka et al. (1985a, 1985b); [d] = Unit-cell volume at 298 K from Chatterjee and Schreyer (1972), thermal expansion of 3.2 × 10^{-5}/°C (Skinner, 1966); [e] = Unit-cell volume at 298 K from Charlu et al. (1978), thermal expansion of 3.3 × 10^{-5}/°C (Cameron and Papike, 1980).

Geothermometry based on the present model results in temperatures that are very similar to those given by the model of Carlson and Lindsley (1988) at pressures below 30 kbar, and are only slightly higher (10–30 °C) at 40–60 kbar. However, as pointed out by Davidson et al. (1988), the model of Carlson and Lindsley (1988) failed to predict the stability of pigeonite in the pyroxene quadrilateral at Fe/(Fe + Mg) of 0.1–0.3 and hence is unsuitable for use in the multicomponent systems. On the other hand, the model of Davidson et al. (1988) cannot be used for the thermobarometry of garnet peridotites and lherzolites at pressures higher than 30 kbar. Only the two-pyroxene thermometry based on the present model is applicable at any pressure in either simple or complex systems.

The model is unique in its ability to predict the phase relations involving protopyroxene, including the phase relations determined by Carlson (1988) at 1 bar and 1295–1425 °C. Thus, the conclusion of Carlson et al. (1988) that the orthopyroxene-like phase at 1 bar and high temperatures is identical to ordinary orthopyroxene is confirmed. The model predicts the stability of all enstatite polymorphs. This includes the newly discovered stability field of high clinoenstatite below the melting curve, previously thought to be metastable with respect to melting. A number of apparent inconsistencies among experimental studies, arising from incomplete understanding of the phase relations in the enstatite-diopside system, is explained.

Perhaps the most important contribution of the model is in its ability to predict the compositions of two coexisting pyroxenes at 100–160 kbar. Although this may not be relevant to thermometry, it is essential for deciphering the mineral and chemical composition and the evolution of the Earth's upper mantle. Gasparik (1990) used the model for calculating the phase relations in the system CaO-MgO-Al_2O_3-SiO_2 (CMAS) for the whole upper mantle. The CMAS system gives a very satisfactory approximation of the complex natural compositions found in mantle xenoliths in terms of predicting the stability of mineral phases and the correct phase relations. It is likely that the CMAS system is an equally good analogue for the whole mantle, and thus essential for estimating its mineral and chemical composition.

The compositions of two coexisting pyroxenes on the CMAS solidus are important in the processes that led to the differentiation of the upper mantle. Herzberg et al. (1990) determined the compositions of the coexisting orthopyroxene, clinopyroxene, and garnet at 100 kbar and 2080 °C in close agreement with the model. From these compositions, they were able to deduce that the melting of a chondritic mantle is peritectic: the composition of the melt is outside the triangle formed by the compositions of the coexisting orthopyroxene, clinopyroxene, and garnet. Hence, the melting of the three-phase assemblage produces peritectic melt and additional orthopyroxene. The peritectic melt could evolve into the peridotitic compositions observed in mantle xenoliths only by separation from the orthopyroxene residue and subsequent fractional crystallization of clinopyroxene and garnet. The compositions of the two coexisting pyroxenes play a crucial role in these processes.

Acknowledgment

This study was funded by NSF grant EAR 86-17550 to the author.

References cited

Anastasiou, P., and Seifert, F. (1972) Solid solubility of Al_2O_3 in enstatite at high temperatures and 1–5 kb water pressure. Contributions to Mineralogy and Petrology, 34, 272–287.

Atlas, L. (1952) The polymorphism of $MgSiO_3$ and solid-state equilibria in the system $MgSiO_3$-$CaMgSi_2O_6$. Journal of Geology, 60, 125–147.

Berman, R.G., and Brown, T.H. (1985) Heat capacity of minerals in the system Na_2O-K_2O-CaO-MgO-FeO-Fe_2O_3-Al_2O_3-SiO_2-TiO_2-H_2O-CO_2: Representation, estimation, and high temperature extrapolation. Contributions to Mineralogy and Petrology, 89, 168–183.

Biggar, G.M. (1988) Protoenstatite compositions from 1 bar to 5 kb (abs.). Chemical Geology, 70, 3.

Boyd, F.R., and England J.L. (1965) The rhombic enstatite-clinoenstatite inversion. Carnegie Institution of Washington Year Book, 64, 117–120.

Boyd, F.R., England, J.L., and Davis B.T.C. (1964) Effects of pressure on the melting and polymorphism of enstatite, $MgSiO_3$. Journal of Geophysical Research, 69, 2101–2109.

Brey, G., and Huth, J. (1984) The enstatite-diopside solvus to 60 kbar. Proceedings of the Third International Kimberlite Conference, 2, 257–264.

Brousse, C., Newton, R.C., and Kleppa, O.J. (1984) Enthalpy of formation of forsterite, enstatite, akermanite, monticellite and merwinite at 1073 K determined by alkali borate solution calorimetry. Geochimica et Cosmochimica Acta, 48, 1081–1088.

Cameron, M., and Papike, J.J. (1980) Crystal chemistry of silicate pyroxenes. In C.T. Prewitt, Ed., Pyroxenes. Mineralogical Society of America Reviews in Mineralogy, 7, 5–92.

Carlson, W.D. (1985) Evidence against the stability of orthoenstatite above ~1005°C at atmospheric pressure in CaO-MgO-SiO_2. Geophysical Research Letters, 12, 409–411.

——— (1986) Reversed pyroxene phase equilibria in CaO-MgO-SiO_2 at one atmosphere pressure. Contributions to Mineralogy and Petrology, 92, 218–224.

——— (1988) Subsolidus phase equilibria on the forsterite-saturated join $Mg_2Si_2O_6$-$CaMgSi_2O_6$ at atmospheric pressure. American Mineralogist, 73, 232–241.

Carlson, W.D., and Lindsley, D.H. (1988) Thermochemistry of pyroxenes on the join $Mg_2Si_2O_6$-$CaMgSi_2O_6$. American Mineralogist, 73, 242–252.

Carlson, W.D., Swinnea, J.S., and Miser, D.E. (1988) Stability of orthoenstatite at high temperature and low pressure. American Mineralogist, 73, 1255–1263.

Charlu, T.V., Newton, R.C., and Kleppa, O.J. (1978) Enthalpy of formation of some lime silicates by high-temperature solution calorimetry, with discussion of high pressure phase equilibria. Geochimica et Cosmochimica Acta, 42, 367–375.

Chatillon-Colinet, C., Newton, R.C., Perkins, D., and Kleppa, O.J. (1983) Thermochemistry of $(Fe^{2+},Mg)SiO_3$ orthopyroxene. Geochimica et Cosmochimica Acta, 47, 1597–1603.

Chatterjee, N.D., and Schreyer, W. (1972) The reaction enstatite+sillimanite=sapphirine+quartz in the system MgO-Al_2O_3-SiO_2. Contributions to Mineralogy and Petrology, 36, 49–62.

Chen, C.-H., and Presnall, D.C. (1975) The system Mg_2SiO_4-SiO_2 at pressures up to 25 kilobars. American Mineralogist, 60, 398–406.

Davidson, P.M., Lindsley, D.H., and Carlson, W.D. (1988) Thermochemistry of pyroxenes on the join $Mg_2Si_2O_6$-$CaMgSi_2O_6$: A revision of the model for pressures up to 30 kbar. American Mineralogist, 73, 1264–1266.

Gasparik, T. (1984) Experimentally determined stability of clinopyroxene + garnet + corundum in the system CaO-MgO-Al_2O_3-SiO_2. American Mineralogist, 69, 1025–1035.

——— (1989) Transformation of enstatite-diopside-jadeite pyroxenes to garnet. Contributions to Mineralogy and Petrology, 102, 389–405.

——— (1990) Phase relations in the transition zone. Journal of Geophysical Research, 95, 15751–15769.

Gasparik, T., and Newton, R.C. (1984) The reversed alumina contents of orthopyroxene in equilibrium with spinel and forsterite in the system MgO-Al_2O_3-SiO_2. Contributions to Mineralogy and Petrology, 85, 186–196.

Grover, J.E. (1972) The stability of low-clinoenstatite in the system $Mg_2Si_2O_6$-$CaMgSi_2O_6$ (abs.). Transactions of the American Geophysical Union, 53, 539.

Herzberg, C., Gasparik, T., and Sawamoto, H. (1990) Origin of mantle peridotite: Constraints from melting experiments to 16.5 GPa. Journal of Geophysical Research, 95, 15779–15803.

Kiseleva, I.A., Ogorodova, L.P., Topor, L.P., and Chigareva, O.G. (1979) Thermochemical studies of CaO-MgO-SiO_2 system. Geokhimiya, 1979, 1821–1825.

Krupka, K.M., Robie, R.A., Hemingway, B.S., Kerrick, D.M., and Ito, J. (1985a) Low-temperature heat capacities and derived thermodynamic properties of anthophyllite, diopside, enstatite, bronzite, and wollastonite. American Mineralogist, 70, 249–260.

Krupka, K.M., Hemingway, B.S., Robie, R.A., and Kerrick, D.M. (1985b) High-temperature heat capacities and derived thermodynamic properties of anthophyllite, diopside, dolomite, enstatite, bronzite, talc, tremolite, and wollastonite. American Mineralogist, 70, 261–271.

Kushiro, I., Yoder, H.S., Jr., and Nishikawa, M. (1968) Effect of water on the melting of enstatite. Geological Society of America Bulletin, 79, 1685–1692.

Lindsley, D.H., and Dixon, S.A. (1976) Diopside-enstatite equilibria at 850 to 1400°C, 5–35 kbars. American Journal of Science, 276, 1285–1301.

Lindsley, D.H., Grover, J.E., and Davidson, P.M. (1981) The thermodynamics of the $Mg_2Si_2O_6$-$CaMgSi_2O_6$ join: A review and an improved model. In R.C. Newton, A. Navrotsky, and B.J. Wood, Eds., Thermodynamics of minerals and melts, p. 149–175. Springer-Verlag, New York.

Mori, T., and Green, D.H. (1975) Pyroxenes in the system $Mg_2Si_2O_6$-$CaMgSi_2O_6$ at high pressure. Earth and Planetary Science Letters, 26, 277–286.

——— (1976) Subsolidus equilibria between pyroxenes in the CaO-MgO-SiO_2 system at high pressures and temperatures. American Mineralogist, 61, 616–625.

Newton, R.C., Charlu, P.A., Anderson, P.A.M., and Kleppa, O.J. (1979) Thermochemistry of synthetic clinopyroxenes in the join $CaMgSi_2O_6$-$Mg_2Si_2O_6$. Geochimica et Cosmochimica Acta, 43, 55–60.

Nickel, K.G., and Brey, G. (1984) Subsolidus orthopyroxene-clinopyroxene systematics in the system CaO-MgO-SiO_2 to 60 kbar: A re-evaluation of the regular solution model. Contributions to Mineralogy and Petrology, 87, 35–42.

Pacalo, R.E.G., and Gasparik, T. (1990) Reversals of the orthoenstatite-clinoenstatite transition at high pressures and high temperatures. Journal of Geophysical Research, 95, 15853–15858.

Perkins, D., and Newton, R.C. (1980) The compositions of coexisting pyroxenes and garnet in the system CaO-MgO-Al_2O_3-SiO_2 at 900–1100°C and high pressures. Contributions to Mineralogy and Petrology, 75, 291–300.

Perrotta, A.J., and Stephenson, D.A. (1965) Clinoenstatite: High-low inversion. Science, 148, 1090–1091.

Presnall, D.C., and Gasparik, T. (1990) Melting of enstatite ($MgSiO_3$) from 10 to 16.5 GPa and the forsterite (Mg_2SiO_4)–majorite ($MgSiO_3$) eutectic at 16.5 GPa: Implications for the origin of the mantle. Journal of Geophysical Research, 95, 15771–15777.

Redlich, O., and Kister, A. T. (1948) Thermodynamics of nonelectrolyte solutions. Algebraic representation of thermodynamic properties and the classification of solutions. Industrial and Engineering Chemistry, 40, 345–348.

Riecker, R.E., and Rooney, T.P. (1967) Deformation and polymorphism of enstatite under shear stress. Geological Society of America Bulletin, 78, 1045–1054.

Robie, R.A., Hemingway, B.S., and Fisher, J.R. (1978) Thermodynamic properties of minerals and related substances at 298.15 K and 1 bar (10^5 Pascals) pressure and at higher temperatures. United States Geological Survey Bulletin, 1452, Washington, D.C.

Ross, N.L., and Navrotsky, A. (1988) Study of the $MgGeO_3$ polymorphs (orthopyroxene, clinopyroxene, and ilmenite structures) by calorimetry, spectroscopy, and phase equilibria. American Mineralogist, 73, 1355–1365.

Schweitzer, E. (1982) The reaction pigeonite = $diopside_{ss}$ + $enstatite_{ss}$ at 15 kbar. American Mineralogist, 67, 54–58.

Sclar, C.B., Carrison, L.C., and Schwartz, C.M. (1964) High-pressure stability field of clinoenstatite and the orthoenstatite-clinoenstatite transition (abs.). Transactions of the American Geophysical Union, 45, 121.

Skinner, B.J. (1966) Thermal expansion. In S.P. Clark, Ed., Handbook of physical constants, p. 75–96. Geological Society of America Memoir, 97, New York.

Smith, J.V. (1969) Magnesium pyroxenes at high temperature: Inversion in clinoenstatite. Nature, 222, 256–257.

Smyth, J.R. (1974) The high temperature crystal chemistry of clinohypersthene. American Mineralogist, 59, 1069–1082.

Stephenson, D.A., Sclar, C.B., and Smith, J.V. (1966) Unit cell volumes of synthetic orthoenstatite and low clinoenstatite. Mineralogical Magazine, 35, 838–846.

Warner, R.D., and Luth, W.L. (1974) The diopside-orthoenstatite two-phase region in the system $CaMgSi_2O_6$-$Mg_2Si_2O_6$. American Mineralogist, 59, 98–109.

Yamada, H., and Takahashi, E. (1984) Subsolidus phase relations between coexisting garnet and two pyroxenes at 50 to 100 kbar in the system CaO-MgO-Al_2O_3-SiO_2. In J. Kornprobst, Ed., Kimberlites. II: The mantle and crust-mantle relationships, p. 247–255. Elsevier, Amsterdam.

Yamamoto, K., and Akimoto S. (1977) The system MgO-SiO_2-H_2O at high pressures and temperatures—Stability field for hydroxyl-chondrodite, hydroxyl-clinohumite and 10 Å-phase. American Journal of Science, 277, 288–312.

Manuscript received May 22, 1989
Manuscript accepted July 6, 1990